

Mixing properties of a shallow basin due to wind-induced chaotic flow

Margit Pattantyús-Ábrahám^{a,*}, Tamás Tél^b, Tamás Krámer^a, János Józsa^a

^a *Department of Hydraulic and Water Resources Engineering, Budapest University of Technology and Economics, Műegyetem rkp 3. K. mf 4, H-1111 Budapest, Hungary*

^b *Institute for Theoretical Physics, Eötvös University, Pázmány Péter stny 1/A, H-1117 Budapest, Hungary*

Received 11 July 2007; received in revised form 25 October 2007; accepted 6 November 2007

Available online 17 November 2007

Abstract

As important environmental features, mixing properties of inland water bodies in unsteady flow conditions are investigated. Time-dependent motion, often resulting in chaotic behavior, requires the Lagrangian description of the transport. As a simple example, unsteady hydrodynamics driven by periodical wind forcing in a simplified shallow lake geometry is considered to explore the main chaotic properties. In the modelled flow field methods identifying strong and weak shearing sub-regions are proposed and applied as mixing indicators. These include the determination and inter-comparison of the finite size Lyapunov exponents (FSLE), the residence time, and the implementation of the so-called leaking method. Coherent structures as stable and unstable manifolds are also identified, playing the role of Lagrangian barriers that hinder local transversal material transfer, and avenues that significantly channel transport. The primary effect of turbulent diffusion on the FSLE fields is also demonstrated.

© 2007 Elsevier Ltd. All rights reserved.

Keywords: Chaotic advection; Manifolds; FSLE; Residence time; Leaking; Diffusion

1. Introduction

In shallow environmental flows horizontal mixing is of particular importance. Its understanding and accurate modeling are essential for applied sciences, such as estimating water exchange mechanisms, interpreting plankton movement or planning and operating pollutant outfalls. Mixing in water takes place due to two main processes: diffusion and advection. The role of diffusion alone is usually minor in the efficiency of mixing, but its combined effect with advection or even more, the complexity of advection in itself can also result in large-scale spreading. In time-dependent velocity fields the basic mechanism is chaotic advection, which is best handled as inherently Lagrangian transport as shown by Aref [2]. With methods originating in chaos theory we are able to locate spatial structures which govern the flow

and areas where the most effective mixing occurs. Such structures as hyperbolic (also called saddle) points and manifolds (see Fig. 1) have long been used for classifying the evolution of trajectories in abstract dynamical systems (for an introduction see e.g. [20]). Their application in the context of fluid dynamics, in turn offers a new tool with clear physical meaning: identifying vortex boundaries, barriers and avenues of transport, or lines of strong stretching [5,8,16]. Especially, chaotic dynamics are characterized by complex intersection of stretching and contracting manifolds around the hyperbolic points. Mixing is typically strong in these regions: trajectories of initially close particles are quickly separated along the stretching directions.

Hyperbolic points are the Lagrangian analogs of Eulerian stagnation points. As is well known, a stagnation point is the intersection of streamlines at a certain instant of time (Fig. 1A). If the flow field were frozen, the fluid would be motionless at such points. As the definition implies, the stagnation point is an instantaneous property of the flow. A hyperbolic point is, on the contrary, a point moving with the fluid, along a periodic orbit in temporally periodic flows.

* Corresponding author. Tel.: +36 1 4631495; fax: +36 1 463 1879.

E-mail addresses: pattantyus@vit.bme.hu (M. Pattantyús-Ábrahám), tel@general.elte.hu (T. Tél), kramer@vit.bme.hu (T. Krámer), jozsa@vit.bme.hu (J. Józsa).

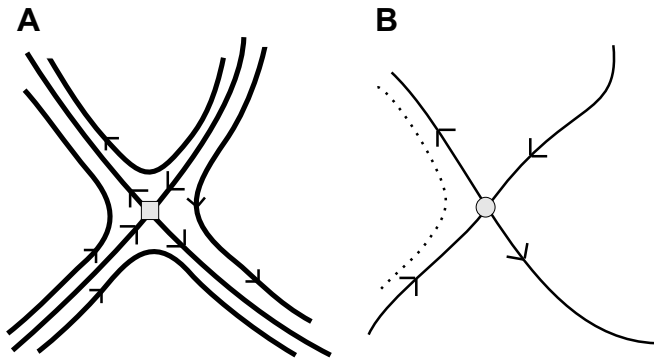


Fig. 1. Schematic illustration of a stagnation point (gray square), which is an instantaneous Eulerian property of the flow (A) and a hyperbolic point (gray dot), also called saddle point, a Lagrangian property carrying information about the long-time properties of the advection dynamics (B). In (A) and (B) the solid lines represent streamlines and the stable and unstable manifolds (the contracting and stretching curves), respectively. The dashed line corresponds to a typical particle trajectory, moving off but close to the manifolds. Such particles spend long time around the hyperbolic point, but eventually escape it. This shows that the periodic orbits corresponding to hyperbolic point are unstable.

At any instant of time there is a curve running towards the hyperbolic point. This curve is the set of all points which, when followed at integer multiples of the period of the flow, will hit the hyperbolic point in the future. This curve can be called the curve of contraction, or, in terms of dynamical system theory, the stable manifold [20] (see Fig. 1B). Similarly, another curve can be defined, the stretching curve or unstable manifold, along which points leave an infinitesimally small neighborhood of the hyperbolic point. The unstable manifold can also be considered as the stable manifold in the time-reversed Lagrangian dynamics. Near hyperbolic points, the rate of separation of nearby particles is exponential. The manifolds of the hyperbolic point reflect the entire history of the fluid around the hyperbolic point. Stagnation and hyperbolic points are thus basically different, although both are surrounded by a cross-like pattern, as seen in Fig. 1. (They coincide in stationary flows only.) Often they happen to be close to each other, as we shall illustrate in the present paper.

In our work we compare different Lagrangian methods, with special emphasis on the finite size Lyapunov-exponent (FSLE) method, the residence time distribution and the leaking method, which have not been applied earlier in inland water context. We take a simple wind-forced shallow basin model, analyze the mixing properties and, in particular, the locations with strong chaotic behavior responsible for efficient mixing. All this reveals new aspects in understanding and interpreting mixing processes in shallow wind-forced lakes, providing additional tools to the water resources management in such an environment.

2. The hydrodynamical model

In order to investigate the chaotic features in a simple, but realistic case, a shallow, wind-forced sample lake was

chosen with dimensions close to the ones typical for shallow inland waters. Representing, e.g., small reed-enclosed inner ponds of shallow lakes (as can be found in the Everglades, or in Lake Neusiedl in Central Europe) while keeping the shape as simple as possible, a horizontally $2 \text{ km} \times 2 \text{ km}$ square-shaped lake was set up. Apart from the nearshore zone, the bottom of such bays usually slopes gently toward the middle, which, nevertheless, can be the reason of significant topographic gyres in the circulation pattern. Thus the depth of the lake was set to 2.5 m in the middle and 2 m all along the shoreline, with linear depth transition for simplicity (Fig. 2).

The lake is forced by a wind speed with 10 m/s North and East components, and the direction is abruptly changed at every 4 h from this NE to a NW direction and vice versa, similarly to Kranenburg's analytical [11], and Liang's numerical models [13,14], where chaos theory for shallow water bodies has been applied. All this results in a highly unsteady periodic flow field (of period $T = 8 \text{ h}$) after the simulation has run sufficiently long. Trajectory computations are started at the first windturn to the NE direction once the flow solution has become periodic. In the paper, model time t always refers to the trajectory computations. As was shown by field measurements and verified by detailed turbulence modeling [9], in such a spatial extension the wind and the surface wind shear stress as the external forcing field presents a systematic irregular distribution governed by the development of the so-called internal boundary layer over the water surface. The near-surface wind and the resulting shear stress field was estimated by considering the development of this layer. Its dependence on the fetch is implemented by simple semi-empirical formulae, justified both by field data and numerical modeling.

As a combined effect, shallow lakes with such depths and wind shear stresses are characterized by strong horizontal circulation patterns [6], thus even a 2D depth-integrated approach can reasonably capture the essentials of horizontal water mass advection, and depth-averaged flow velocities may be applied to describe water exchange mechanisms. In order to do so, the numerical solution was obtained by a standard two-dimensional, depth-integrated shallow water model. We assumed a uniform Manning bed roughness $n = 0.025 \text{ s/m}^{1/3}$ and in view of the moderate extent, the effect of the Earth's rotation is neglected. The governing equations are in terms of the conservative variables (depth and volume flux components), and these variables are arranged on a uniform, Cartesian grid of 40 m cell size according to the Arakawa C layout [1]. No normal flow is allowed along the shoreline and a perfect-slip boundary condition is imposed for the tangential flux component. To achieve second-order accuracy in space, spatial derivatives are approximated by central differences, except in the advective terms which are upwinded. The solution is advanced in time using an explicit Euler-type method whose timestep is limited by the Courant stability condition [12].

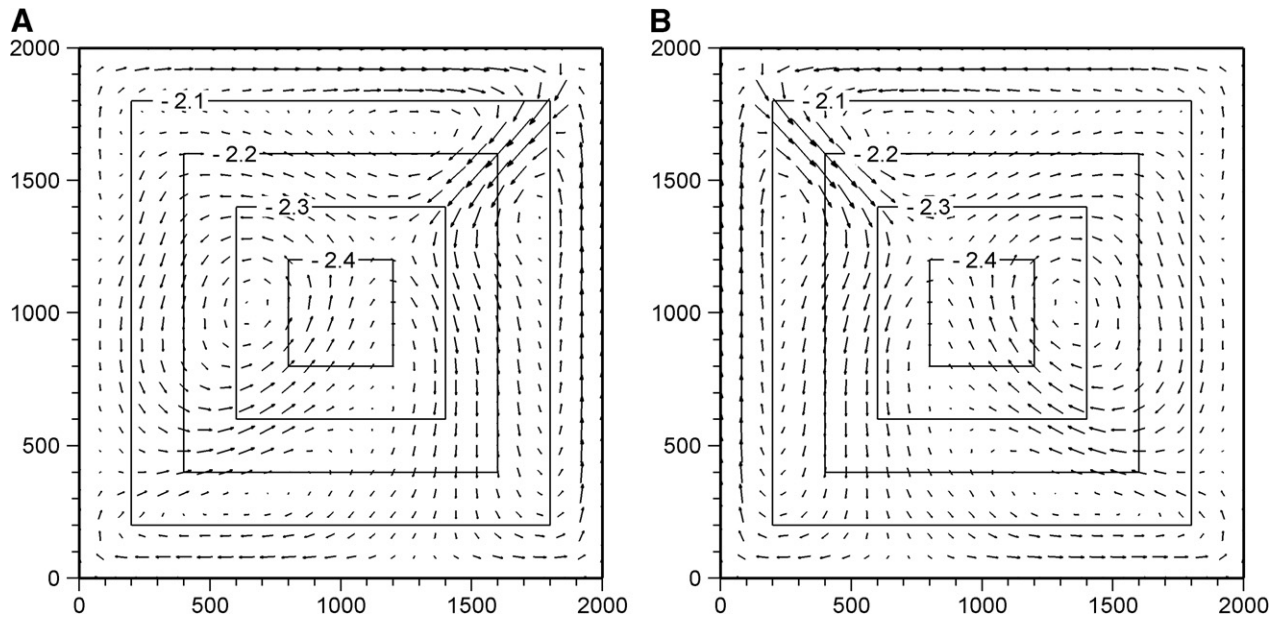


Fig. 2. The bathymetry contours and the velocity field (arrows) of the model-lake at $t = 0$ (A) and $t = 1/2T = 4\text{h}$ (B). Longest arrows indicate flow velocity close to 10 cm/s. The horizontal and vertical axis corresponds to the x and y axis, respectively.

3. Lagrangian methods and traditional approaches for chaos analysis

The Eulerian velocity components are provided on the aforementioned grid at discrete time steps of 600 s. Particle positions are calculated using velocity fields with East and North components $u(x, y, t)$, $v(x, y, t)$ linearly interpolated between time steps t_i and t_{i+1} at intermediate time level t to obtain the Lagrangian particle paths. The advection equations

$$\frac{dx}{dt} = u(x, y, t), \quad \frac{dy}{dt} = v(x, y, t)$$

were solved by a fourth-order Runge–Kutta scheme using bilinear spatial interpolation. The solution of these equations in time-dependent flows is typically chaotic. Fig. 3 demonstrates typical trajectories.

In panel A a chaotic trajectory is exhibited. This particle gets into the vicinity of particles of different origin, therefore effective mixing between diverse water bodies takes place along the entire trajectory. Originally compact fluid parcels become here very strongly stretched and folded. The region visited by the trajectory in panel B is smaller, the trajectory itself is non-chaotic. This particle is followed by the surrounding tracers, and mixing is only able to occur due to diffusion. Such a region corresponds to badly mixed dead zones where fluid parcels are weakly distorted only, and compact patches remain compact as time goes on. Panel B also contains a special trajectory, a closed unstable periodic orbit. The orbit becomes closed after a single period of the flow; it is a period-one orbit. Points of this orbit are hyperbolic points. (Stable periodic orbits can also exist in the lake; they are typically the midpoints of the dead zones.) It is instructive to see a comparison of the instanta-

neous Lagrangian pattern around the hyperbolic point and the Eulerian pattern around the corresponding stagnation point of the flow (Fig. 4).

4. Leaking advection dynamics

A novel way of visualizing mixing properties is provided by the method of “leaking” introduced by Schneider et al. [17] (see also [18,19,22]). This method is based on monitoring particles which do not enter a pre-selected area, the leak, over very long times. If the advection dynamics is chaotic, the monitored particles trace out fractal patterns (see Fig. 5). The starting position of these particles indicates the so-called stable manifold, from where they reach hyperbolic points. Their end positions locate the unstable manifolds, along which the hyperbolic points are left. The midpoint of these trajectories must be close (cf. Fig. 1B) to the hyperbolic points (see also [20]). The main message of Fig. 5 is that there is an infinity of hyperbolic orbits outside the leak (the chaotic saddle, in dynamical systems terminology). One of them is, of course, the hyperbolic orbit of Figs. 3B and 4B, but there are infinitely many more. Most of the corresponding trajectories become, however, closed after more than one period only. The set of hyperbolic points forms a fractal set, and so do their manifolds.

Note that the precise pattern depends on the size and location of the leak. The smaller the leak, the denser the set of hyperbolic points and its dimension approaches two. This indicates that in the original, unleased system the hyperbolic points are space filling. Simultaneously, the manifolds also shade a fluid area. The manifolds of the leaked problem provide thus a subset of the full stable or unstable foliation of the closed system.

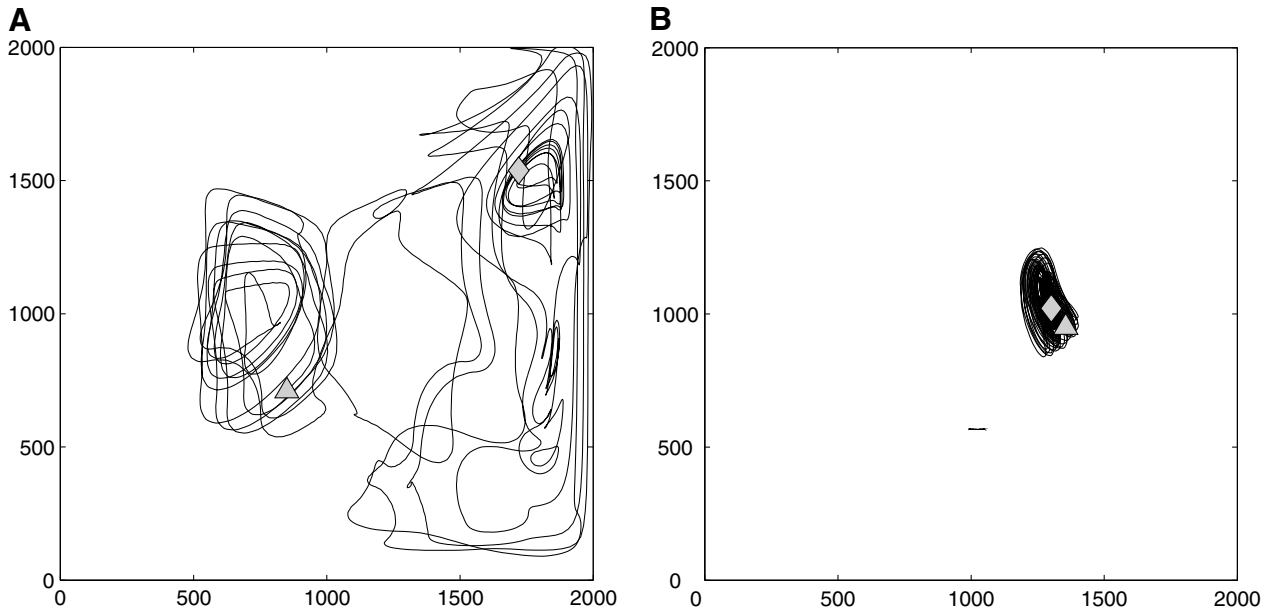


Fig. 3. Particle trajectories started at time zero from $x = 900$ m, $y = 760$ m (panel A) and $x = 1405$ m, $y = 960$ m (panel B), simulated over 15 periods (120 h). Initial and end positions are marked by a gray triangle and diamond, respectively. The qualitatively different trajectories indicate strongly and weakly mixing regions of the lake. In panel B an unstable periodic orbit (closed curve, appears on the figure as a short dash at $x = 1017$ m, $y = 566$ m) is also indicated.

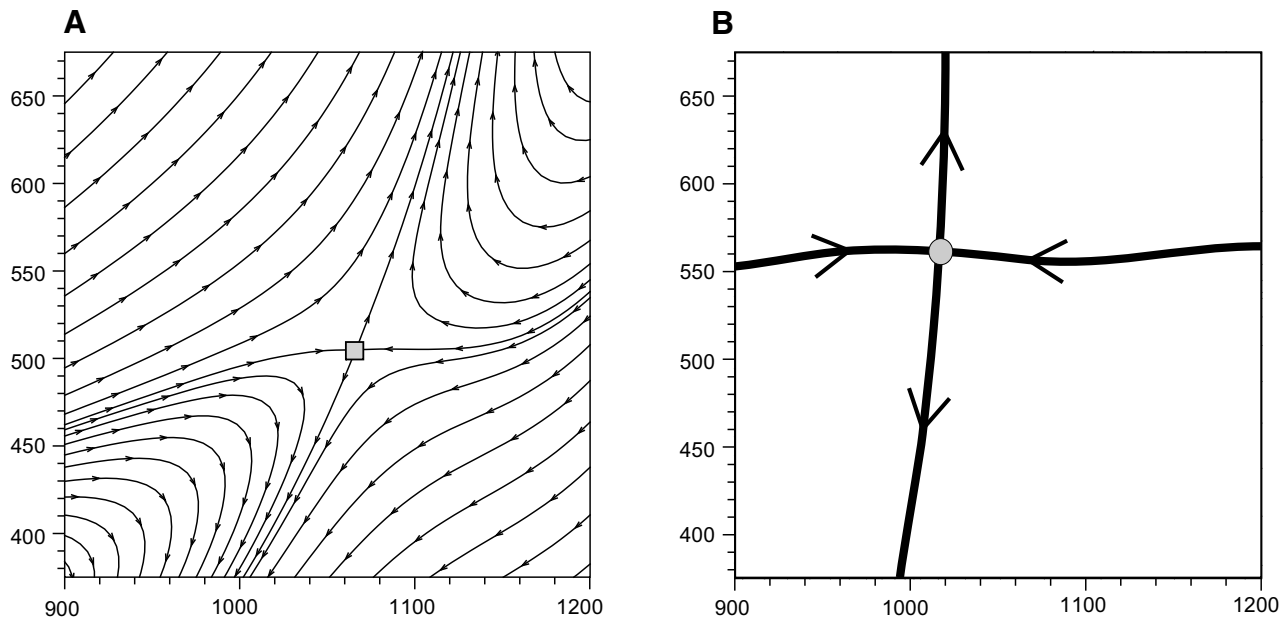


Fig. 4. Streamlines around a stagnation point (gray square) of the hydrodynamical model presented in Section 2 (A), and a nearby hyperbolic point (gray dot) (B) along with its stable and unstable manifolds (the way to determine these manifolds will be shown later). The pictures are valid at integer multiples of the period T of the flow. The coordinates (in m) of the stagnation and hyperbolic points are (1070, 504) and (1017, 566), respectively.

It is worth complementing the leaking picture by showing those particles, which go out of the rectangle. In principle, all points outside the stable manifold leave the rectangle after sufficiently long times. One gets, however, additional information if target regions are defined outside and the initial locations are colored according to the first arrival to these regions. To mimic a problem relevant in environmental pollution prevention, we choose these

regions as bands (of width 100 m) along the four shores of the lake. The result is shown in Fig. 6¹ and indicates that hazards released in the rectangle at time zero are most dangerous for the southern shore, which may be alarming in case popular beaches happen to be there. The eastern and

¹ For interpretation of color in Figs. 6, 7 and 9–16, the reader is referred to see the web version of this article.

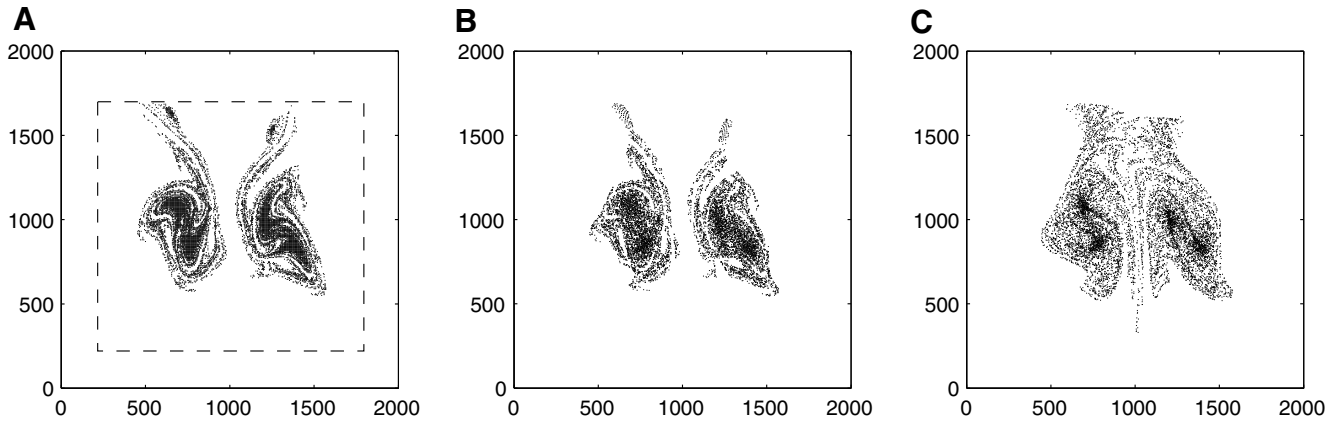


Fig. 5. Stable manifold (A), the set of all hyperbolic points (B) and the unstable manifold (C) of the leaked advection dynamics. The leak is the complement set of the rectangle $200 < x < 1800$ m, $200 < y < 1700$ m, a region along the shores of the lake. The figures are based on uniformly distributing 150,000 initial points over the aforementioned rectangle and keeping only those trajectories originating from these points which do not enter the leak over 52 periods. The points in panels A, B and C are obtained as the initial point at $t = 0$, the midpoint at time $t = 26T = 208$ h, and the endpoint at $t = 52T = 516$ h of these trajectories, respectively. The dashed line in panel A represents the inner boundary of the leak (the outer boundary is the shoreline).

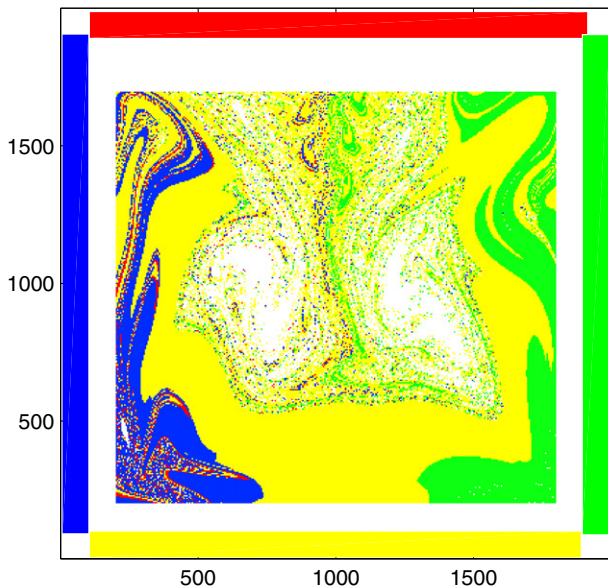


Fig. 6. Initial condition of points of the rectangle which reach target regions inside the leak during 30 periods (10 days). The leak is the same as in Fig. 5. Target regions: 100 m wide bands along the west, north, east and south shore marked as light gray (blue), black (red), gray (green) and dark gray (yellow), respectively. Points ending outside these bands in the leak, or remaining inside the rectangle, are marked with white. White regions and regions in which all four colors accumulate correspond to the stable manifold of Fig. 5A, since this object corresponds to the never escaping initial conditions.

western shores are somewhat less polluted, while the northern shore remains practically intact. Perhaps the most striking feature is the highly interwoven boundary between different colors. A well-known analog of this in dissipative systems is the phenomenon of fractal basin boundaries [20].

A related fingerprint of the advection dynamics can be obtained by choosing a small hole in the (unleaked) flow and identifying those points of the fluid surface which enter this hole over a long period of time (Fig. 7). The set of these

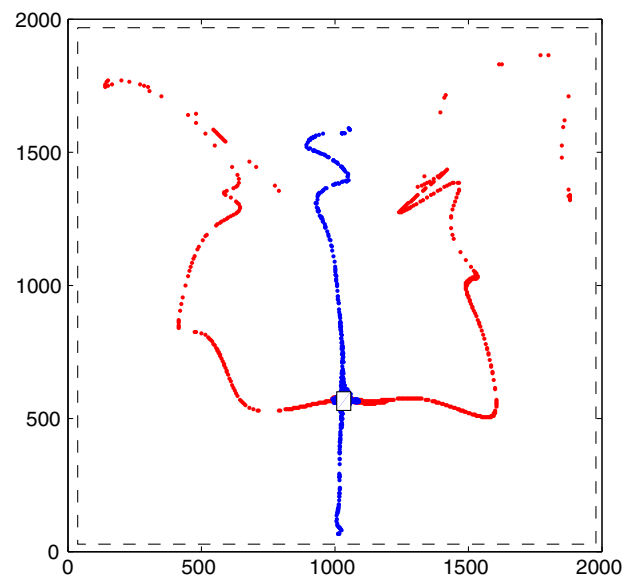


Fig. 7. Initial positions in light gray (red) and end positions in black (blue) of particles which traverse the hole $1025 \leq x \leq 1040$ m, $560 \leq y \leq 590$ m (white rectangle) at any time within eight periods (10 days), started at time zero ($t = 0$) from region $50 \leq x \leq 1950$ m, $50 \leq y \leq 1950$ m (dashed rectangle). These curves are also fractal-like, and indicate the chaoticity of the advection dynamics.

points can be called the collecting zone of the hole (a kind of stable manifold). Similarly, the points flowing out of the hole trace out another set, the target zone (which is the collecting zone of the time-reversed advection dynamics). The complicatedly folded structure of both zones is a clear manifestation of chaos in the problem.

5. Finite size Lyapunov exponents

The leaking method is unable to provide a quantitative measure of the strength of particle separation. The traditional way to characterize this feature is the determination

of the standard Lyapunov exponent of chaotic advection (see e.g. [20]). This is defined as the average exponential rate of separation of initially nearby fluid parcels, averaged over long times. The concept of finite size Lyapunov exponent (FSLE) has been developed as a generalisation of the average Lyapunov exponent by Aurell et al. [3] (see also [5]) in order to study non-asymptotic dispersion processes in the absence of any leak. This quantity has been used for detecting and visualizing Lagrangian structures (transport barriers and vortex boundaries) and analyzing dispersion processes both in the atmosphere [10] and in the ocean [16].

The FSLE technique consists of using a set of tracers with an initially small separation, δ_0 . These tracers are then simultaneously advected by integrating the velocity field. For a chaotic system the separation is known to grow exponentially in time. The FSLE at position \mathbf{x} and time t is computed from the time τ the particle needs to reach separation δ_f from a moving reference particle as

$$\lambda(\mathbf{x}, t, \delta_0, \delta_f) \equiv \frac{1}{\tau} \ln \frac{\delta_f}{\delta_0}. \quad (1)$$

Fig. 8 illustrates diagrammatically the meaning of FSLE. Large FSLE values mark regions in which the particle is faced with strong stretching in its future. As is well known [20], it is the extremely (exponentially) strong stretching and the unavoidable folding occurring in the flow which is a basic feature of chaotic dynamics. The FSLE marks thus the local strength of exponential separation and, therefore, of chaos.

The FSLE distribution was calculated by tracking 150,000 particles released in the nodes of a regular grid of 5 m resolution. To reduce the grid-induced anisotropy in the FSLE results, the calculations were carried out with the four diagonally adjacent particles. Their average distance was taken as the separation which should reach the final distance δ_f . An example of the FSLE distribution is shown in Fig. 9.

Filamental structures in Fig. 9 mark large values of the FSLE. They correspond to the stable manifold since parti-

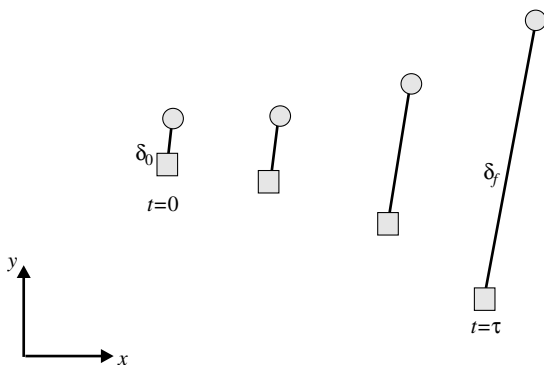


Fig. 8. Schematic diagram of the computation of FSLE. τ is the time needed for two particles (indicated by a dot and square) with initial separation δ_0 to reach the final separation δ_f . The FSLE is the value λ evaluated via Eq. (1).

cle pairs from these regions must have come close to the hyperbolic points during the simulation. As mentioned earlier, the full set of stable manifolds, which is called the stable foliation, traces out a two-dimensional area, but the figure illustrates that manifolds with high values of the FSLE appear to be fractals of dimension less than two. In particular, hyperbolic points of period one (like e.g. the point of Fig. 4B) carry particularly large values of FSLE. It is remarkable that nearby points, if belonging to different filaments, have drastically different (although positive) FSLE values. This sensitive dependence on location is also a determining feature of chaos.

Structures of poor mixing (regions with low FSLE values) can be identified as dark regions (FSLE close to zero). Tori, similar to the one traced out in Fig. 3B, are for instance the bean shaped regions around the middle of the picture.

The amount of detail in the rather convoluted chaotic fields is affected by the grid density of the flow solution. To investigate this dependence, we have repeated the flow simulations on a finer grid (25 m grid size instead of 40 m). The effect of increased resolution is nearly undistinguishable on the contoured flow field. The filaments of the FSLE field computed from the densely resolved flow field are somewhat thinner, sharper and more twisted, but the overall structure of the FSLE field is not affected.

The FSLE distribution, like the results of the previously described methods, depends on time t when the particles are inserted into the flow, as illustrated in Fig. 10. In fact, the bean-shaped regions rotate in time (cf. Fig. 10) and the total area shaded by the bean on the right corresponds to that of the black coil of Fig. 3B.

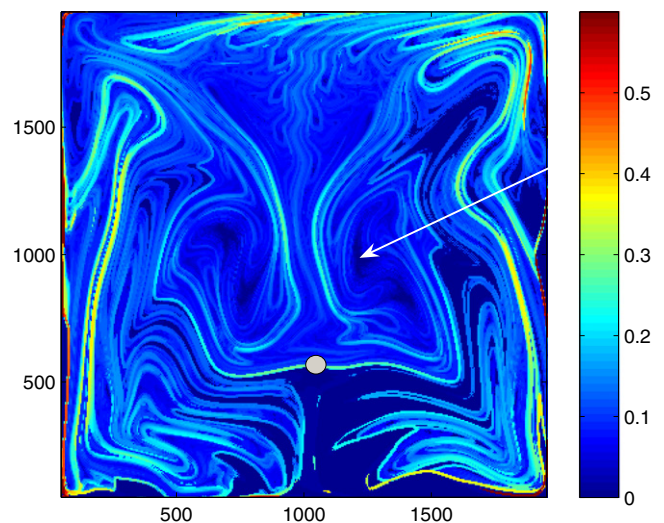


Fig. 9. The FSLE distribution at time $t=0$ in the model lake in $50 \leq x \leq 1950$ m, $50 \leq y \leq 1950$ m obtained with $\delta_0 = 5 \cdot \sqrt{2}$ m, $\delta_f = 250 \cdot \sqrt{2}$ m. The grid spacing of the monitored particles (150,000) is 5 m in both directions. The color bar indicates the FSLE values in $[\text{h}^{-1}]$. The hyperbolic point of Fig. 4B is marked here and in the following figures by a gray dot. The arrow points to the torus mentioned in Fig. 3B.

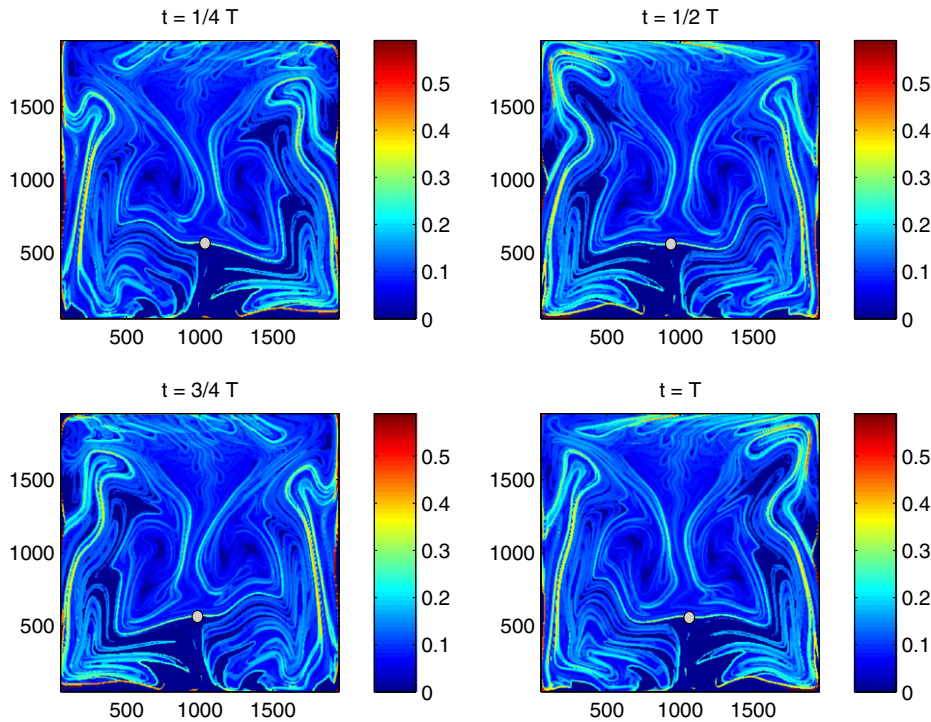


Fig. 10. The FSLE distribution in the model lake at times $t = \frac{1}{4}T$, $t = \frac{1}{2}T$, $t = \frac{3}{4}T$, $t = T$.

To obtain more information about the areas of poor mixing, we propose to use the τ distribution (see Fig. 11). The variable τ denotes the time needed by a particle at (\mathbf{x}, t) to reach the averaged threshold distance δ_f (with δ_0 as initial separation). In our case, two types of poorly mixing areas can be isolated: (i) white (dark red) particles started at $t = 0$ from this area stay together over the full simulation period (25 days), (ii) light gray (yellow and red) particles that stay together for a period longer than 15–25 days.

Particle trajectories can be computed also backward in time after reversing the velocity vectors. The resulting backward FSLE distribution produces similar filamental structures, as can be seen in Fig. 12. The filaments mark the unstable foliation. The full unstable foliation is again space filling, but those of high FSLE values are fractals. In particular, the filaments appearing in gray (yellow) and white (red) mark the unstable manifold of the hyperbolic point. The dark areas locate poorly mixed regions.

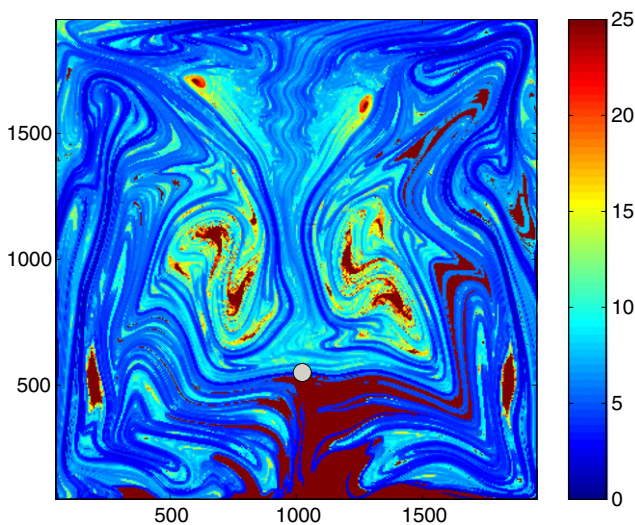


Fig. 11. The distribution of τ in days at $t = 0$. The initial condition of particles is the same as in Fig. 9.

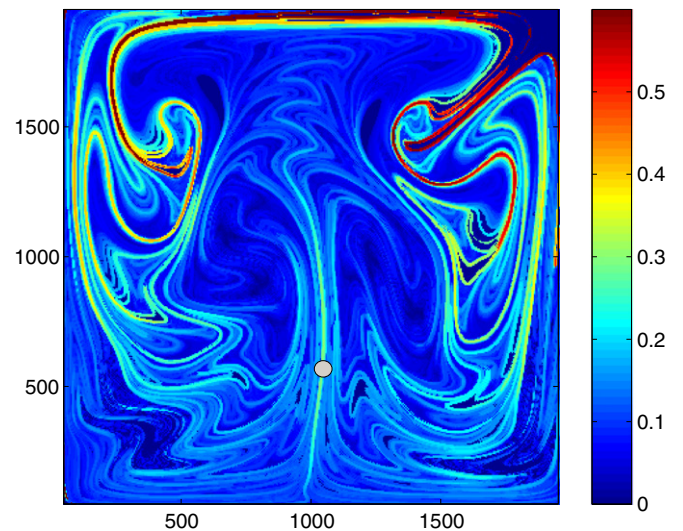


Fig. 12. The FSLE distribution in the backward advection dynamics in $[h^{-1}]$ at $t = 0$. The initial condition is the same as in Fig. 9.

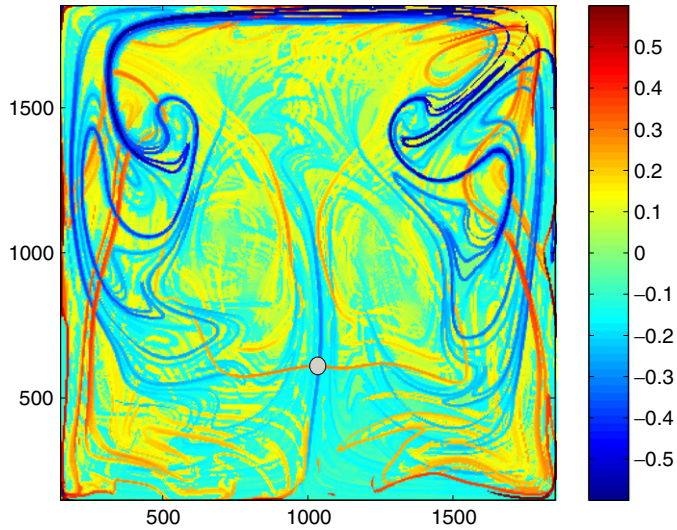


Fig. 13. Combined plot of the forward and backward FSLEs in $[\text{h}^{-1}]$ at $t=0$. The initial conditions of particles are the same as in Fig. 9. Backward FSLEs are indicated with negative values.

The combination of the FSLE distribution of both the forward and backward dynamics is shown in Fig. 13. At a given point of the lake the FSLE of greater absolute value is shown, and the forward (backward) computed FSLE values are marked as positive (negative) numbers. The several intersections of the stable and unstable manifolds confirm in this representation, too, the existence of a huge number of hyperbolic points.

Fig. 14 indicates an interesting feature of the FSLE plots. By a mere change of the color coding we can wash out minor details and concentrate on the most striking patterns. We introduce a threshold, and FSLE values smaller than this threshold are shaded as if the FSLE were zero. As the threshold increases, regions of small FSLEs are merged to a single

domain and the shading enhances the most important manifolds. This representation clearly selects the stable and unstable manifolds (in white (red) and black (blue), respectively) of the main period-one hyperbolic points. The method works obviously in temporally aperiodic flows as well. It provides then an alternative for determining the finite-time stable and unstable manifolds of hyperbolic points which is much easier to apply numerically than the method developed by Haller, as can be seen in [7,23,15].

Finally we compare the residence time plot obtained by the leaking method with the FSLE distribution of the unleaked problem (Fig. 15). Initial positions of quickly escaping particles are indicated in black (blue) in Fig. 15A. Regions from where particles have longer residence time (i.e. take longer to escape) are shaded gray (green and yellow). Particles that remain within the pre-selected rectangle throughout the observed period are marked white (red). Since particles close to the unstable manifold existing within the rectangle leave the box quickly but particles close to the stable manifold stay in the pre-selected region for a long time, areas with long residence time visualize the stable manifolds. They can also indicate coherent structures like tori. Particles in such regions never cross the boundary towards the leak and never escape. As a consequence, the same bean-shaped regions appear in light gray (red) in Fig. 15A as in the corresponding FSLE distribution (Fig. 15B). In general, the patterns well inside the boxes are the same, but those around the edges differ. The reason is that particles around the edges quickly escape and cannot, therefore, contribute to long residence times.

6. The effect of diffusion on FSLE

We devote this section to estimating the effect of turbulent diffusion on the filamentary patterns of the advection

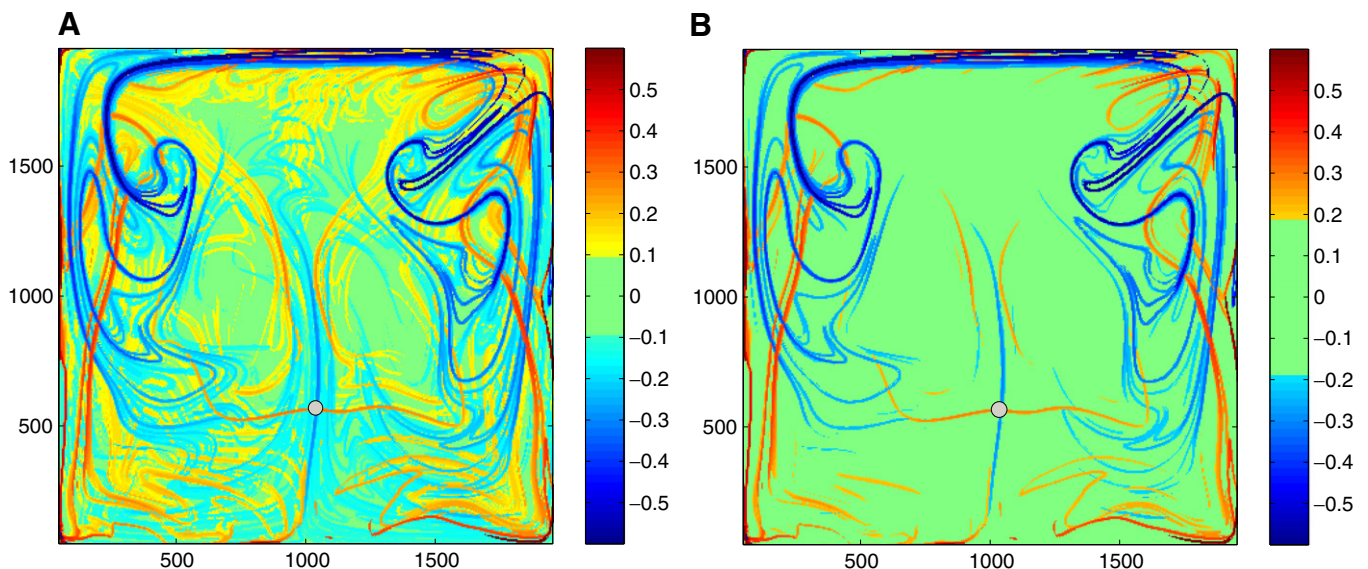


Fig. 14. Enhancing the most pregnant manifolds, by applying threshold shading on the combined plot of the forward and backward FSLEs of Fig. 13. The threshold values are 0.10 (A) and 0.2 h^{-1} (B).

dynamics. Assume that a dye is distributed in a band along an unstable manifold. The width of this band will slowly increase due to diffusion. The growth would go on without any limitation if the flow were not present. The permanent stretching along the unstable manifold is, however, accompanied with a contraction across the unstable manifold. This contraction will slow down the diffusive spreading and the two effects will eventually lead to a finite bandwidth δ around the manifold. The precise time dependence of the bandwidth has been derived by Tél et al. [21]. A detailed analysis is beyond the scope of this paper, here we just quote that the steady-state bandwidth is determined by the diffusivity coefficient D and the average Lyapunov exponent λ as

$$\delta = \sqrt{\frac{D}{\lambda}} \tag{2}$$

The existence of this quantity as a characteristic length is obvious from dimensional considerations as well.

The average Lyapunov exponent is estimated from the FSLE-s of Fig. 9 to be $\lambda = 0.3 \text{ h}^{-1}$. With a turbulent diffusivity of $0.1 \text{ m}^2/\text{s}$ we obtain δ approx 30 m. This implies that the use of a grid size of 5 m was too fine in the presence of such a diffusivity. A realistic picture mimicking the effect

of diffusion can therefore be obtained by averaging out the FSLE values on the original grid over boxes of about six times larger in linear size. The result is shown in Fig. 16A. The picture is of course less detailed than in Fig. 9, but the basic patterns remain the same, similarly as showed for noisy dynamical systems by Ben-Mizrachi et al. [4].

Interestingly, the investigation of how the FSLE results depend on the choice of the initial and final separation leads to a similar conclusion. First note that Eq. (1) suggests that $\lambda(\mathbf{x}, t, \delta_0, \delta_f)$ depends essentially on the ratio δ_f per δ_0 . Thus a decrease of δ_f corresponds to an increase of δ_0 , i.e. to the choice of a coarser resolution. By taking δ_f six times smaller than in the original case, we obtain indeed a similar distribution, shown in Fig. 16B, as via the direct averaging method motivated by presence of the turbulent diffusivity in Fig. 16A.

7. Conclusions

Mixing properties of inland water bodies were studied in an essentially Lagrangian framework. As chaos-induced properties, coherent structures such as manifolds and hyperbolic points were determined. In a simplified shallow

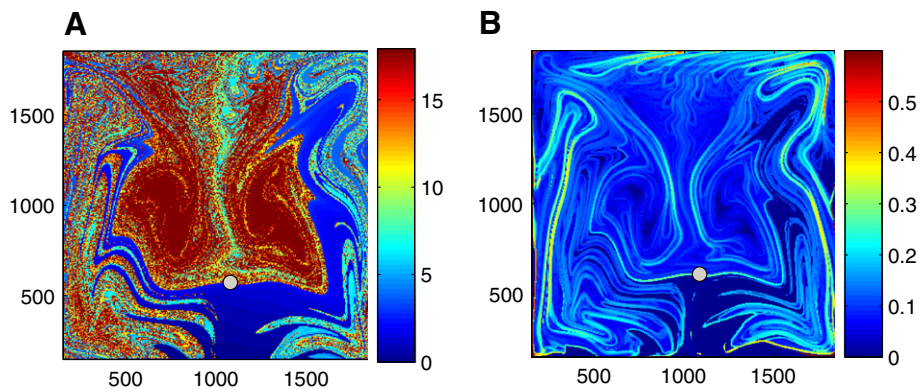


Fig. 15. Panel A: Residence time (in days) up to 18 days within the rectangle outside the leak. The leak is the complement set of the rectangle in Fig. 7. Panel B: The FSLE distribution for the same area taken from Fig. 9.

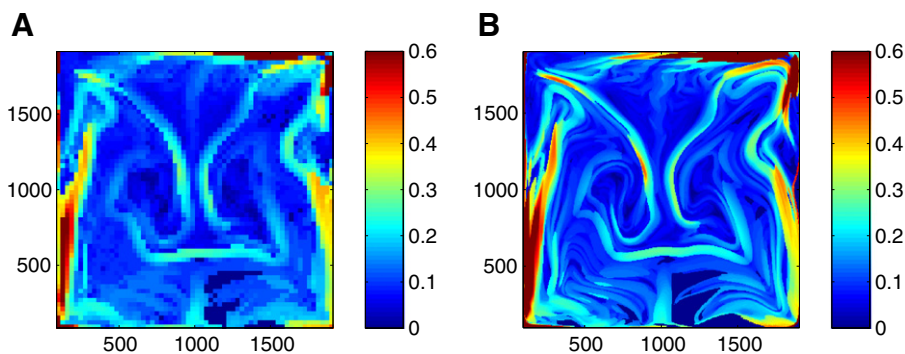


Fig. 16. Panel A: FSLE distribution in the presence of turbulent diffusion of $D = 0.1 \text{ m}^2/\text{s}$. The plot is technically obtained by averaging out Fig. 9 over a grid of linear size of 30 m. Panel B: The FSLE distribution calculated with $\delta_f = 42 \cdot \sqrt{2} \text{ m}$, six times smaller than in Fig. 9 for the same area.

lake geometry unsteady hydrodynamics driven by periodical wind forcing was considered and the focus was on exploring the main chaotic mixing properties. In the numerically modeled depth-averaged flow field methods identifying strong and weak shearing sub-regions and visualizing various parameter fields as mixing indicators were applied and compared to each other. This included the determination and inter-comparison of the finite size Lyapunov exponents (FSLE) and the residence time, playing an important role in hydrobiology, as well as the implementation of the so-called leaking method. These fields made then possible to find important process governing elements such as stable and unstable manifolds which play the role of Lagrangian barriers hindering local transversal material transfer, and avenues that significantly channel transport in the inherently unsteady advective flow field. The primary effect of turbulent diffusion on the FSLE fields was also demonstrated through properly changing the δ_f per δ_0 ratio. Assigning a realistic value to the diffusion coefficient the large-scale flow structures did not change significantly, only somewhat smeared the fine thin stripes in the FSLE distribution.

As to a first practical relevance in environmental and hydraulic engineering, the chaos related findings presented here can facilitate to explain discrepancies found between real-life behavior of pollutants and conventional mixing theories. Furthermore, it underlines the importance of applying Lagrangian techniques in mixing analyzes in general, and in highly unsteady surface flows in particular.

Acknowledgement

This research was supported by the OTKA Grants T047233 and TS044839.

References

- [1] Arakawa A, Lamb VR. Computational design of the basic dynamical processes of the UCLA general circulation model. In: Chang J, editor. *General circulation models of the atmosphere, methods in computational physics: advances in research and applications*. San Francisco: Academic Press; 1977. p. 173–265.
- [2] Aref H. Stirring by chaotic advection. *J Fluid Mech* 1984;143:1–21.
- [3] Aurell E, Boffetta G, Crisanti A, Paladin G, Vulpiani A. Predictability in the large: an extension of the concept of Lyapunov exponent. *J Phys A* 1997;30:1–26.
- [4] Ben-Mizrachi A, Procaccia I, Grassberger P. Characterization of experimental (noisy) strange attractors. *Phys Rev A* 1984;29:975–7.
- [5] Boffetta G, Lacorata G, Redaelli G, Vulpiani A. Detecting barriers to transport: a review of different techniques. *Physica D* 2001;159:58–70.
- [6] Curto G, Józsa J, Napoli E, Krámer T, Lipari G. Large scale circulations in shallow lakes. In: Brocchini M, Trivellato F, editors. *Advances in fluid mechanics. Vorticity and turbulence effects in fluid structure interactions*, vol. 45. Southampton, United Kingdom: Westex Institute of Technology Press; 2006. p. 83–104.
- [7] Haller G. Finding finite-time invariant manifolds in two-dimensional velocity fields. *Chaos* 2000;10:99–108.
- [8] Iudicone D, Lacorata G, Rupolo V, Santoleri A, Vulpiani A. Sensitivity of numerical tracer trajectories to uncertainties in OGCM velocity fields. *Ocean Modell* 2002;4(3):313–25.
- [9] Józsa J, Milici B, Napoli E. Numerical simulation of internal boundary-layer development and comparison with atmospheric data. *Bound-Lay Meteorol* 2007;123:159–75.
- [10] Koh T-Y, Legras B. Hyperbolic lines and the stratospheric polar vortex. *Chaos* 2002;12(2):382–94.
- [11] Kranenburg C. Wind-driven chaotic advection in a shallow model lake. *J Hydraul Res* 1992;30:29–46.
- [12] Krámer T, Józsa J, Sarkkula J. Modelling of a coastal wetland for restoration planning. In: *Proceedings of the symposium on restoration of lakes and wetlands*, November 2000, Bangalore, India.
- [13] Liang Q, Borthwick AGL, Taylor PH. Wind-induced chaotic advection in shallow flow geometries. Part I: Circular basins; Part II: Non-circular basins. *J Hydraul Res* 2006;44:170–9. 180–8.
- [14] Liang Q, Taylor PH, Borthwick AGL. Particle mixing and reactive front motion in unsteady open shallow flow – modelled using singular value decomposition. *Comput Fluids* 2007;36:248–58.
- [15] Mathur M, Haller G, Peacock T, Ruppert-Felsot JE, Swinney HL. Uncovering the Lagrangian skeleton of turbulence. *Phys Rev Lett* 2007;98:144502.
- [16] d’Ovidio F, Fernández V, Hernández-García E, López C. Mixing structures in the Mediterranean Sea from finite-size Lyapunov exponents. *Geophys Res Lett* 2004;31:L17203. doi:10.1029/2004GL020328.
- [17] Schneider J, Tél T, Neufeld Z. Dynamics of “leaking” Hamiltonian systems. *Phys Rev E* 2002;66:066218.
- [18] Schneider J, Tél T. Extracting flow structures from tracer data. *Ocean Dyn* 2003;53:64–72.
- [19] Schneider J, Fernández V, Hernández-García E. Leaking method approach to surface transport in the Mediterranean Sea from a numerical ocean model. *J Marine Syst* 2005;57:111–26.
- [20] Tél T, Gruiz M. *Chaotic dynamics, an introduction based on classical mechanics*. Cambridge University Press; 2006.
- [21] Tél T, De Moura A, Grebogi C, Károlyi G. Chemical and biological reactions in open flows: a dynamical system approach. *Phys Rep* 2005;413:91–196.
- [22] Tuval I, Schneider J, Piro O, Tél T. Opening up fractal structures of three-dimensional flows via leaking. *Europhys Lett* 2004;65:633–9.
- [23] Voth GA, Haller G, Gollub JP. Experimental measurements of stretching fields in fluid mixing. *Phys Rev Lett* 2002;88:254501.